Thin Solid Films 588 (2015) 19–25

Contents lists available at ScienceDirect

Thin Solid Films

journal homepage: www.elsevier.com/locate/tsf

Enhanced charge transport properties by strengthened necks between TiO_2 aggregates for dye sensitized solar cells

Kwangsuk Park [a], Qifeng Zhang [b], Junting Xi [b], Guozhong Cao [b,*]

[a] Gangwon Regional Division, Korea Institute of Industrial Technology, Gangneung-Si, Gangwon-Do 210-340, Republic of Korea
[b] Department of Materials Science and Engineering, University of Washington, Seattle, WA 98195, USA

ARTICLE INFO

Article history:
Received 16 October 2014
Received in revised form 10 April 2015
Accepted 17 April 2015
Available online 24 April 2015

Keywords:
Electrochemical impedance spectroscopy
Scattering
Aggregates
Dye sensitized solar cells

ABSTRACT

The electron diffusion in the TiO_2 aggregate network was enhanced through the addition of TiO_2 nanoparticles with preferential filling at the necks between adjacent TiO_2 aggregates, which resulted in strengthening the connections, while retaining the porous structure of the TiO_2 network. The fortified necks was found to reduce the transport resistance (R_t) by allowing facile transfer of electrons from one aggregate to another, while the scattering effect of the TiO_2 aggregate network got weakened with adding the TiO_2 nanoparticles as a result of reduction of the light scattering centers such as the necks and gaps between the aggregates. However, due to the increase in surface area as the TiO_2 nanoparticles were added, the diminished light scattering effect of the aggregate network was compensated and even the highest performance was achieved when the 10% TiO_2 nanoparticle was added into the TiO_2 aggregate film, suggesting that widening necks between sub-micrometer sized light scatters such as an aggregate would be a good strategy in achieving further improvement of power conversion efficiency of dye sensitized solar cells through the improved charge transport property.

1. Introduction

Since the achievement of the breakthrough in dye sensitized solar cells (DSCs) that used a TiO_2 mesoporous film on which monolayered dye molecules are adsorbed in 1991, nanostructured semiconducting oxide materials have been intensively studied by varying materials and their shapes because an oxide mesoporous network plays a significant role in determining performance of DSCs [1,2] and[3]. A mesoporous structure made of nanoparticles is believed not the best for a photoanode due to its random and highly grained surface and boundary structures, which impede electron transport and/or escalate charge recombination. However, the high surface area for monolayered dye molecules adsorbed on a nanostructured network is required to generate as high as 20 $mAcm^{-2}$ as a result of good light harvesting and electron injection [4,5]. On the other hand, high susceptibility of recombination resulting from the high surface area must be suppressed by a characteristic feature of DSCs; spatial and physical separation between photocarrier generation and transport [5].

TiO_2 nanoparticles with ~20 nm in diameter have been commonly used as an oxide material and the photoanode composed of this oxide network is transparent, indicating that some incident photons that are not absorbed by dye sensitizers just pass through DSCs. This loss of the incident photons can be reduced by adopting light scatters with the size ranging from 300 nm to 1000 nm, leading to the increase of light absorption in the region of 500 nm [6,7]. There are two ways in applying scattering particles; double-layer structure and aggregate form. The former one can be achieved by depositing a scattering layer on top of the nanoparticle layer, in which each layer has its own role for the improvement of light harvesting efficiency (LHE) [8,9]. The nanoparticle layer is responsible for high surface area and the scattering layer plays a role of a scattering center. The other is a hierarchical aggregate structure which has both roles of a nanoparticle layer and scatter layer due to its characteristic features; sub-micrometer size and mesoporous structure [10,11]. The sub-micrometer size of an aggregate triggers the light scattering and at the same time, its mesoporous structure minimizes the reduction of surface area coming from the aggregation of nanocrystallites. As a result, the TiO_2 aggregate film demonstrated 9% efficiency at 1 sun, which was ascribed to both good light harvesting coming from high internal surface area and light scattering and long diffusion length related with high crystallinity and compact packing of the TiO_2 nanocrystallites [12].

Once electrons are injected into the conduction band of an oxide from the excited dyes, they have to be collected at a conducting substrate through an oxide network, indicating that good electron transport in a nanostructured film plays a great role in achieving high performance of DSCs so a lot of concerns have been focused on 1D structure such as nanorod to improve electron transport property [13,14]. The aggregate structure seems to suffer from electron transport in terms of connections between aggregates [15]. Usually, nanostructured oxides are sintered at the temperature ranging of 350 to 500 °C to form an oxide network that provides pathways for charge transport,

* Corresponding author. Tel: 1 206 616 9084; Fax : 1 206 543 3100.
E-mail addresses: gzcao@u.washington.edu, gzcao@uw.edu (G. Cao).

http://dx.doi.org/10.1016/j.tsf.2015.04.054
0040-6090/

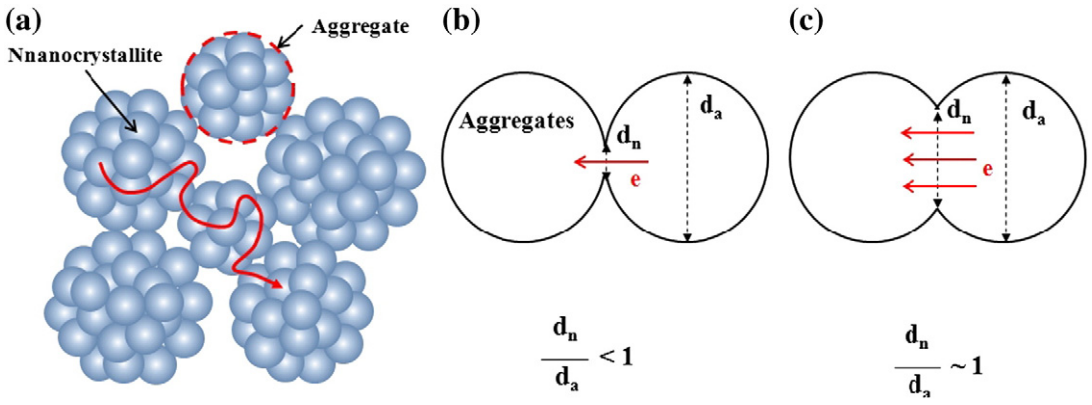

Fig. 1. Schematics illustrating (a) electron diffusion in aggregates and through necks between aggregates, (b) low possibility of electron transfer from one aggregate to adjacent one due to poor neck, and (c) high possibility of electron transfer as a result of widened neck compared to the diameter of the aggregate.

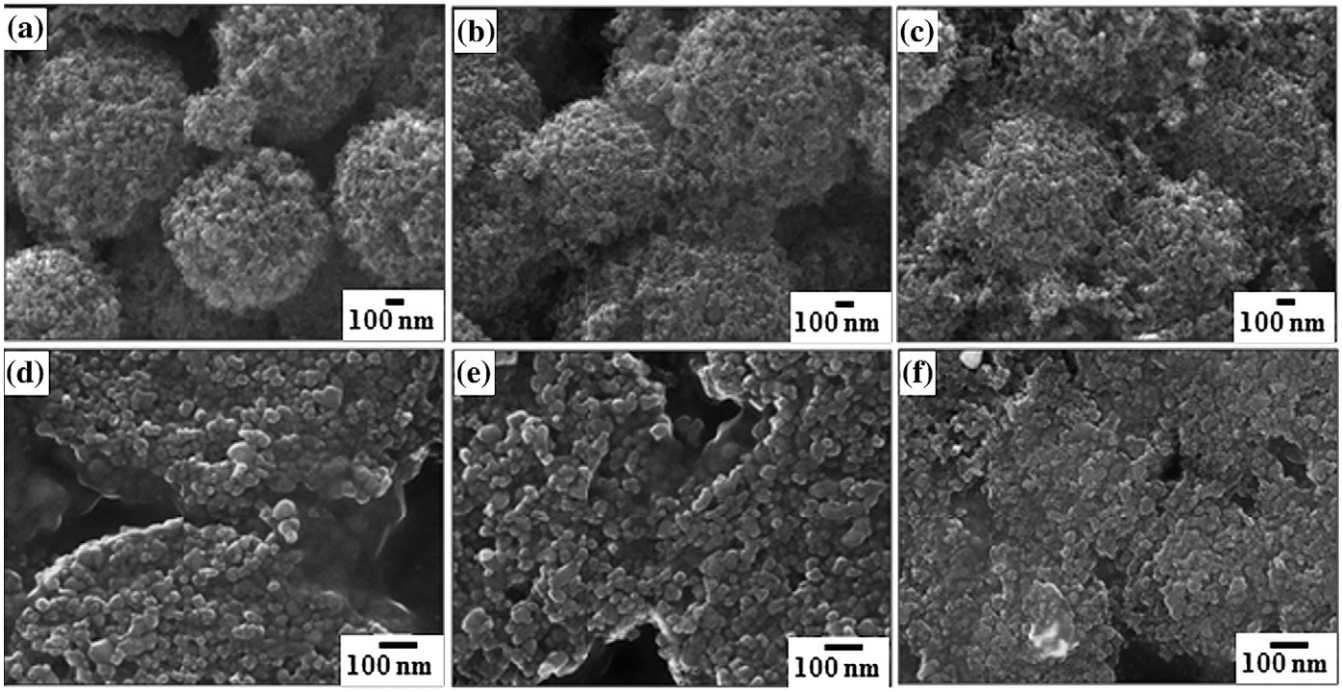

Fig. 2. SEM images showing surface and cross-sectioned morphologies of (a) and (d) Aggregate, (b) and (e) Mix10 and (c) and (f) Mix20 films.

which involves mass flow by diffusion at contacting points between adjacent oxide nanoparticles. In a photoanode made of aggregated nanocrystallites, the electron diffusion occurs not only through numerous nanocrystallites in an aggregate but also through necks between two adjacent aggregates, before reaching fluorine doped tin oxide (FTO) substrate, as shown in Fig. 1(a). Small sized nanocrystallites form more connections per unit space, enabling electrons to diffuse through a nanocrystallite network effectively. However, the submicrometer size and spherical shape of the aggregate limit contacting area between aggregates, leading to the poor connection (neck formation) between the aggregates during sintering. So, the limited contact (neck) between adjacent aggregates would be a bottleneck for charge transport because the narrow neck (d_n) compared to the diameter of an aggregate (d_a) gives less chances to allow electrons to move from one to another aggregate, as shown schematically in Fig. 1(b). Increased neck diameter, as shown in Fig. 1(c), would promote the electron migration from one to adjacent aggregate considerably.

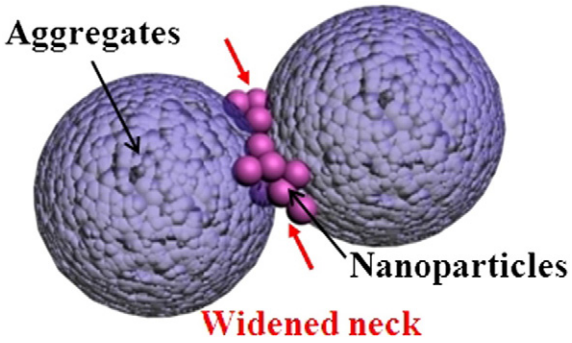

Fig. 3. Schematic showing the widened neck between two aggregates achieved by filling with the added nanoparticles.

The widened neck for better charge transport could be achieved by increasing annealing temperature and/or prolonging annealing time; however, such thermal treatment would unavoidably also introduce negative impacts such as reduced surface area, which will reduce the dye molecule adsorption. This paper proved the poor charge transport

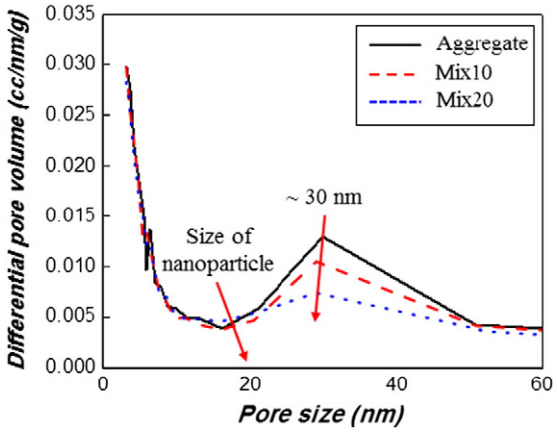

Fig. 4. Pore size distribution of Aggregate, Mix10 and Mix20 films measured by BJH model.

Table 1
Surface areas measured by multi-point BET model for Aggregate, Mix10 and Mix20 films.

	Surface area	Porosity	Dye loading
Aggregate	65 m^2g^{-1}	65.9%	0.077 $mgcm^{-2}$
Mix10	62 m^2g^{-1}	63.6%	0.081 $mgcm^{-2}$
Mix20	64 m^2g^{-1}	61.3%	0.087 $mgcm^{-2}$

in the submicron-sized TiO_2 aggregate network and much improved electron diffusion in the TiO_2 aggregate network with strengthened necks achieved by adding the small sized TiO_2 nanoparticles. The addition of the TiO_2 nanoparticles into the TiO_2 aggregates results in not only the strengthened necks but also additional surface area so electrochemical impedance spectroscopy (EIS) was used to investigate electron transport as well as recombination with the addition of the TiO_2 nanoparticles into the TiO_2 network at the same time.

2. Experimental procedures

2.1. Preparation of TiO_2 aggregates

Submicrometer sized TiO_2 aggregates were fabricated through an electrospray process. Degussa P25 nanoparticles as TiO_2 nanocrystallites were dispersed in water–ethanol solvent (1:1 volume ratio) containing poly(vinylpyrrolidone) (MW $\approx 1.3 \times 10^6$), followed by a stir for 24 h to get a well-dispersed suspension. The suspension was electrosprayed with a flow rate of 0.3 mL/h, keeping the distance and applied voltage between the needle tip of the syringe containing the suspension and the grounded aluminum substrate 17 cm and 12 kV to form the spherical aggregate structure. The needle size was 20 G. The TiO_2 aggregates collected on the grounded aluminum foil were dried at 100 °C for 2 h for effective separation of the TiO_2 aggregate from the aluminum foil.

2.2. Fabrication of solar cells

Doctor blade method was used to make a film on FTO glass. Pastes were prepared by mixing an organic media containing terpineol and ethyl cellulose with TiO_2 aggregates and mixtures of TiO_2 nanoparticles (P25) and aggregates with weight ratios of 0.1:0.9 and 0.2:0.8, respectively (labeled as Aggregate, Mix10 and Mix20). The pastes were coated on FTO glasses via doctor blade to form the TiO_2 films with a thickness of about 10 μm. The films were first dried at 150 °C for 20 min to remove the organic media and then, annealed at 450 °C for 1 h to form the TiO_2 network. The films were sensitized with N719 (Solaronix) by immersing them in an ethanol solution containing 0.3 mM of N719. The sensitized films as a photoanode were assembled with counter electrodes for which platinum-coated silicones were used and the gap between two electrodes was filled with an electrolyte composed of 0.6 M tetrabutylammomium iodide, 0.1 M lithium iodide, 0.1 M iodine and 0.5 M 4-tert-butylpyridine in acetonitrile.

2.3. Characterization

Surface and cross-sectioned morphologies of the films were examined through scanning electron microscopy (SEM, JSM-7000). Brunauer–Emmett–Teller (BET, Quantachrome NOVA 4200e) was used to check variations in surface area and porosity of the films with the addition of TiO_2 nanoparticles into TiO_2 aggregates. UV–Vis spectrophotometer equipped with an integrating sphere was used to determine amount of dye loading and measure absorbance and reflectance of the sensitized electrodes. 0.1 M Na_2SO_4 solution was used to dissolve the dye molecules from the sensitized electrodes. Charge transport properties such as charge transfer resistances (R_{ct}), transport resistances (R_t) and chemical capacitances (C_μ) were characterized by electrochemical impedance spectroscopy (EIS) performed by the Solartron 1287A equipped with the Solartron 1260 FRA/impedance analyzer. Frequency applied ranged from 0.05 to 10^5 Hz, keeping an ac amplitude of 10 mV and forward bias voltages was varied from 0.55 V to 0.75 V. The performance of the solar cells was measured by using a HP 4155A programmable semiconductor parameter analyzer under AM 1.5 simulated sunlight with a power density of 100 mW cm^{-2}.

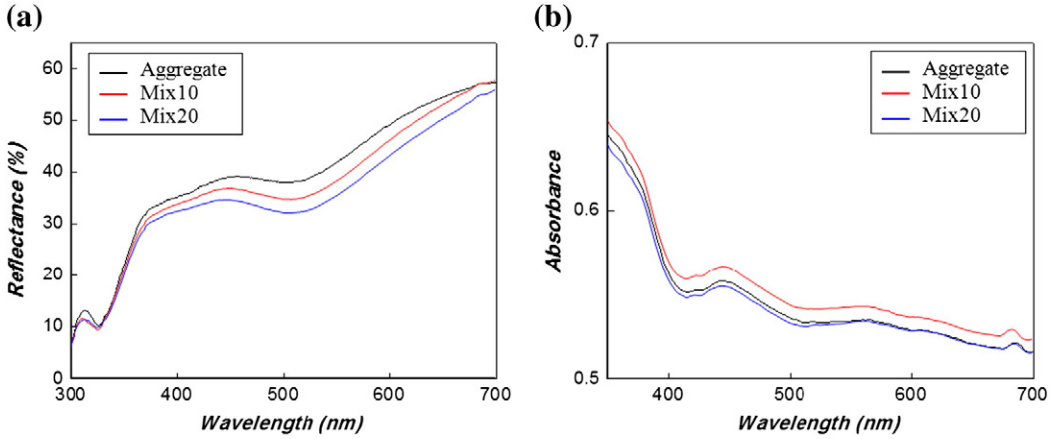

Fig. 5. (a) Reflectance and (b) absorbance spectra of Aggregate, Mix10 and Mix20 photoanodes sensitized with N719.

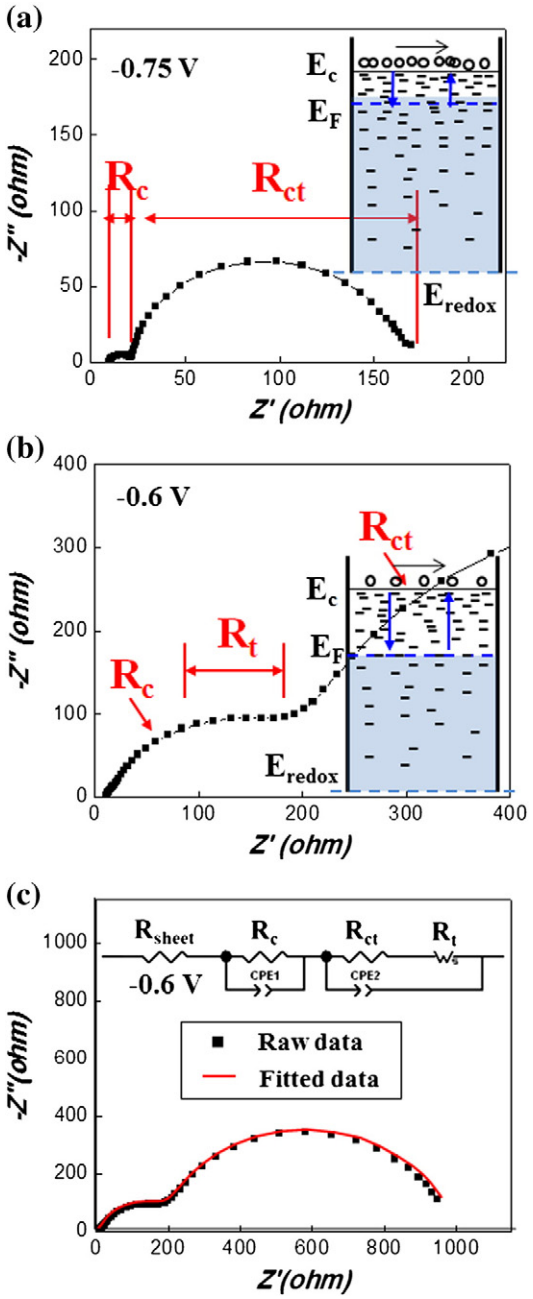

Fig. 6. Nyquist plots of DSCs measured at (a) forward bias open circuit condition, (b) reduced bias voltage from an open circuit condition and (c) fitted result with the equivalent circuit in an inset. Under an open circuit bias voltage (0.75 V), the electron concentration in conduction band is relatively high, resulting in high conductivity (low diffusion resistance), while the low electron concentration in conduction band as a result of the reduced bias voltage (0.6 V) gives rise to the decrease in the conductivity, making transport resistance (R_t) detectable in the Nyquist plot. The black and blue arrows in schematics denote electron diffusion in conduction band and trapping–detrapping process, respectively.

3. Results and discussion

Fig. 2 shows the surface and cross-sectioned morphologies of the films composed of Aggregate, Mix10 and Mix20. As shown in Fig. 2(a), the aggregates in the range of 200–800 nm were well-packed, leaving a lot of open spaces between the aggregates. The contacted area (neck) between adjacent aggregates seems to be small compared to the size of the aggregates. These poor connections were strengthened by simply admixing the aggregates with the nanoparticles, as shown in Fig. 1(b) and (c).

The nanoparticles of 10 wt.% added seemed to fill the necks preferentially, keeping the gaps between aggregates opened. However, further increase of the nanoparticle ratio up to 20 wt.% started to block the gaps, forming big clusters of the aggregates, as shown in Fig. 2(c). The cross-sectioned images of the films gave much clear understanding on the structural variation of the necks between the aggregates with adding the nanoparticles. As shown in Fig. 2(d), there was little connected area at the neck in the aggregate film. The added nanoparticles enriched at or around the neck between the aggregates, making the neck widened, as shown in Fig. 2(e). For Mix20 shown in Fig. 2(f), it is hard to distinguish an aggregate from the others, suggesting that the added nanoparticles filled the most gaps and thus, resulted in the fully connected aggregate film.

Filling this poor neck with nanoparticles could be a good approach in improving connections between aggregates because small size of nanoparticles can be easily inserted into the poor necks and sintered so can make widened pathway between the aggregates, allowing facile transfer of electrons. Fig. 3 shows schematically an improved neck structure of aggregates by adding nanoparticles around a neck, which could be thought to be the similar case with Fig. 1(b).

As electron diffusion in the aggregate network is strongly related to structural parameters of the network such as size and morphology of nanocrystallite, neck structure between particles and even surface area [15,16], it is first needed to confirm the structural changes of the aggregate films when the nanoparticles were added into the aggregates and these were systematically investigated by BET. As denoted in SEM images, the gaps (large pores) around the necks were filled up with the added TiO_2 nanoparticles, indicating that some large pores got disappeared. Fig. 4 shows pore size distribution measured by BJH (Barett–Joyner–Halenda) model. Even though BJH model only provides information on the mesopore region (2–50 nm), the nitrogen sorption results revealed unambiguously that the larger pores than the TiO_2 nanoparticle size (~20 nm) were filled with the added TiO_2 nanoparticles, resulting in the widened necks as observed in Fig. 2. Meanwhile, the pore size distribution below 20 nm did not show any changes with the addition of TiO_2 nanoparticles into the TiO_2 aggregates, supporting the fact that the inside aggregate and nanoparticle network have the same pore structure as P25 was used for both.

Table 1 shows the measured surface area and porosity through multi-point BET model and amount of the dye adsorbed on the TiO_2 films. As expected, the specific surface area of the film (based on the weight of materials) was not considerably affected by the addition of nanoparticles, which is consistent with the previous result that the aggregate and nanoparticle films have similar surface area when the same nanocrystallite (P25) was used for them [17]. However, the decrease in porosity of the film indicates that adding nanoparticles makes the film denser by filling necks and/or large gaps between the aggregates with the added nanoparticles, as observed in Fig. 2. That means that for the film formed on a substrate in a given volume, surface area becomes larger as the TiO_2 nanoparticles are added into the TiO_2 aggregates as a result of the denser packing of the materials. Accordingly, the amount of the dye adsorbed on the film was increased with the addition of the TiO_2 nanoparticles as a result of the increased surface area.

Fig. 5 shows reflectance and absorbance spectra of three photoelectrodes sensitized with N719. One of the structural changes observed in the films, loss of large gaps between the aggregates where light scattering mainly occurs with the addition of the TiO_2 nanoparticles resulted in reduction of reflectance over 400 nm wavelength, indicating that light scattering effect was diminished with adding the TiO_2 nanoparticles, as shown in Fig. 5(a). However, the absorbance results were somewhat different from the reflectance variation with adding the nanoparticles. The aggregate and Mix20 films showed almost same absorbance behavior, while the absorbance of the Mix10 was

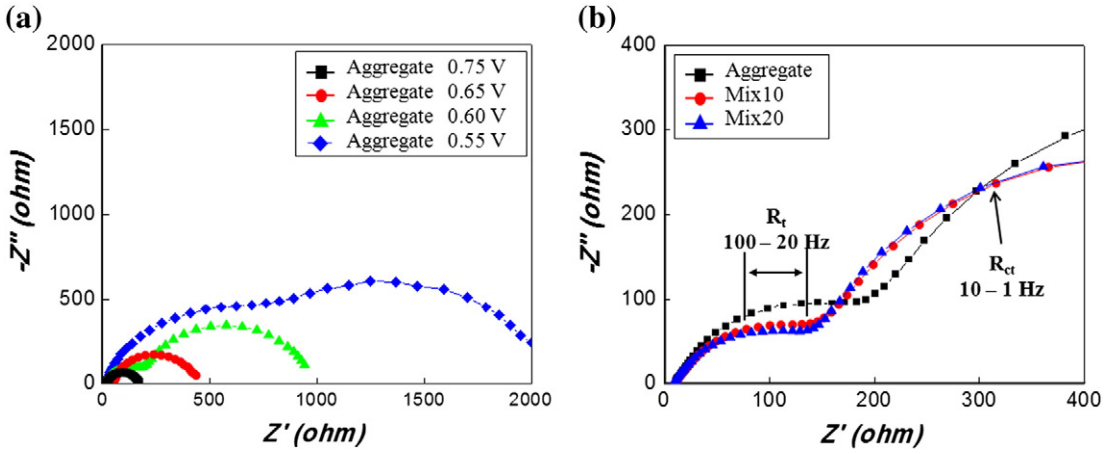

Fig. 7. (a) Variation of Nyquist plots of Aggregate with forward bias voltage and (b) Nyquist plots of Aggregate, Mix10 and Mix20 measured at 0.60 V, showing transport resistances (R_t) in the region of 20–100 Hz.

improved. Absorbance of a sensitized film is thought to be determined by combined contribution between amount of dyes adsorbed on a film and scattering effect (reflectance) of a film. As described before, the added nanoparticles filled necks and/or large gaps between the aggregate where light scattering mainly occurs so reflectance of the film was decreased with the addition of the TiO_2 nanoparticles. On the other hand, the amount of the adsorbed dyes became increased as the TiO_2 nanoparticles were added as a result of the increased surface area in a given volume. That means that there is a compensated characteristic between the reflectance and amount of the adsorbed dyes (surface area) in case of the addition of the TiO_2 nanoparticles into the aggregates, leading to the highest absorbance when the 10 wt.% nanoparticle was added. The similar variation when a composite is formed by mixing nanoparticles and large crystals is also observed in incident photon-to-current efficiency (IPCE), where the concepts of light scattering and dye uptake are used to discuss this phenomenon [18,19].

Electrochemical impedance spectroscopy (EIS) is a well-established technique in characterizing charge transport properties of DSCs because it shows all kinetic processes occurring in DSCs except for electron injection from excited dye molecules such as electron transport and recombination [20,21,22]. Under an EIS measurement, the electrons are injected into an oxide network from a FTO substrate and the oxide network gets charged by propagation of the injected electrons. At the same time, some of the injected electrons in the conduction band of the oxide are recombined with I_3^- ions in a redox electrolyte. Typically, Nyquist plot has three semicircles with frequency ranges, which represent different charge transport processes; charge transfer at counter electrode/electrolyte interface in a range of 10^4–10^3 Hz (R_c), charge transfer at oxide/electrolyte interface around 10^1 Hz (R_{ct}) and ion diffusion in an electrolyte below 10^0 Hz. But, transport resistance (R_t) which be observed in a range of 10^3–10^2 Hz, denoting how effective the electrons in the conduction band of TiO_2 move along with the TiO_2 network, is not usually detected in Nyquist plot at a bias open circuit condition due to the small value compared to other two charge transfer resistances (R_c and R_{ct}) [23]. As the measured electron diffusion is ascribed to the electron movement in the conduction band, relatively high electron concentration in the conduction band under a bias open circuit condition results in low diffusion resistance. Fig. 6(a) is a Nyquist plot in a frequency range of 10^5–10^0 Hz, which just displays two semicircles. The reduced bias voltage causes a decrease of the electron concentration in conduction band, resulting in an increase in transport resistance (R_t), which looks like Warburg-like diffusion, as shown in Fig. 6(b). The Nyquist plots were interpreted with an equivalent circuit, as shown in Fig. 6(c). Even though transmission line model was well developed to analyze Nyquist plot [24,25], a simplified equivalent circuit would be a better fit because all the measurements carried out at 0.55–0.75 V resulted in well-defined regions for each component such as R_c, R_t and R_{ct} [26–28,29].

Fig. 7(a) shows the variation of Nyquist plot with bias voltages for the aggregate photoelectrode. With the reduction of the bias voltage, all resistances such as R_c, R_t and R_{ct} increased, enabling R_t to be distinguishable from R_c and R_{ct}, as discussed above. And it is obvious that the transport resistance (R_t) decreased with the addition of TiO_2 nanoparticles into TiO_2 aggregates, indicating that the widened necks

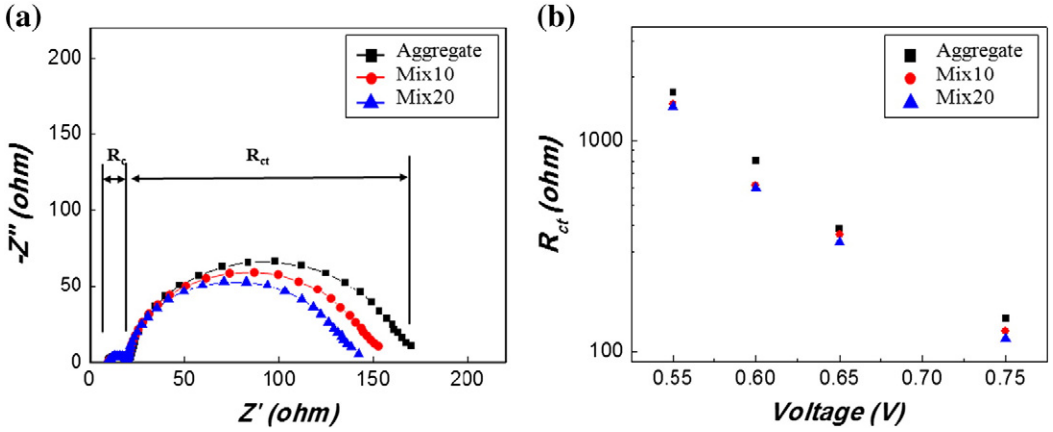

Fig. 8. (a) Nyquist plot of Aggregate, Mix10 and Mix20 films measured at 0.75 V under dark condition and (b) measured charge transfer resistance (R_{ct}) with bias voltage.

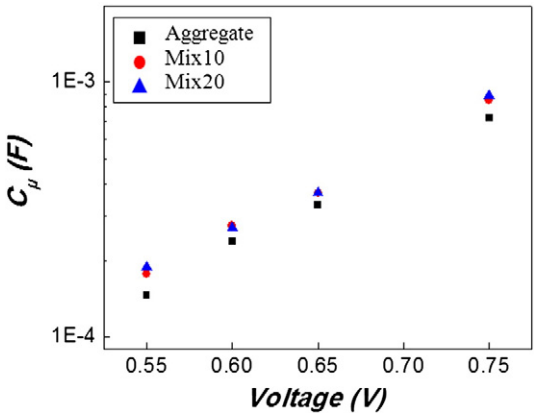

Fig. 9. Chemical capacitance (C_μ) of Aggregate, Mix10 and Mix20 measured at different bias voltages.

through the addition of nanoparticles affected the electron transport, as shown in Fig. 7(b). Interestingly, there was no difference in R_t between samples Mix10 and Mix20. When considering the conditions of a network for electron transport such as neck and coordination number, Mix20 would be expected to have better charge transport than that in Mix10 due to the filled up gaps between adjacent aggregates, which offers better electrons passing. So, the same R_t between Mix10 and Mix20 is likely to mean that there is a saturation point of the charge transport in the nanostructured network.

The addition of TiO_2 nanoparticles into the TiO_2 aggregates not only fortifies the necks between adjacent TiO_2 aggregates but also increases the surface area as the preferential filling of the TiO_2 nanoparticles at the necks between adjacent TiO_2 aggregates makes a TiO_2 aggregate film denser. As the charge recombination occurs at the surface of an oxide network, the change in surface area with adding the nanoparticles would affect recombination kinetics [30,31]. Fig. 8(a) shows a decrease of the charge transfer resistance at TiO_2/electrolyte interface (R_{ct}) as the nanoparticles were added into the aggregates, indicating that Mix10 and Mix20 became more sensitive to recombination than pure aggregate photoanode as a result of the increased surface area. As shown in Fig. 8(b), the exponential dependence of R_{ct} on the bias voltage remained at the bias voltage region studied in this work. The exponential dependence indicates that the electrons from conduction band were trapped at localized states in band gap, and their escape from the localized state (detrapping) governed charge transport properties in the test condition, which is schematically illustrated in Fig. 6. That means that the density of localized states should be considered in analyzing charge

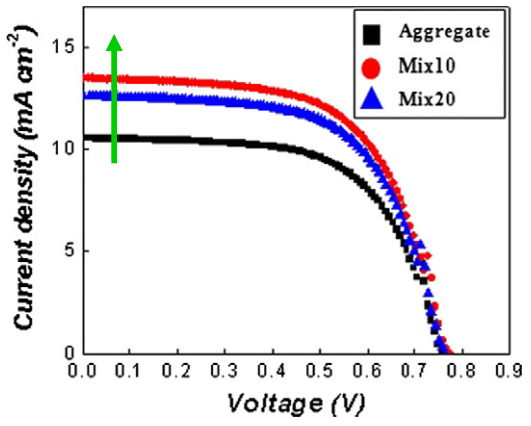

Fig. 10. J–V curves of the DSCs with the photoanodes composed of Aggregate, Mix10 and Mix20 under the illumination with 100 mWcm^{-2}.

transport properties as trapping–detrapping events into/from localized states reduce electron diffusion in conduction band (R_t). Chemical capacitance (C_μ) denoting accumulation of charges (electrons) in an oxide network could be utilized to characterize the density of the localized state because more than 90% of the electrons are trapped in an oxide network and less than 10% of the electron act as free electrons under working condition [32].

Fig. 9 plotted the chemical capacitances of Aggregate, Mix10 and Mix20 calculated from EIS results. With the exponential dependence on the bias voltage, the chemical capacitance (C_μ) was higher in the Mix10 and Mix20 than the pure aggregate photoanode, indicating that new localized states were introduced from the TiO_2 nanoparticles added. It can be assumed that all nanoparticles have the same localized states; the denser structure of Mix10 and Mix20 consists more nanoparticles and so has higher C_μ than that of Aggregate. The increased localized states reduce electron movement in a particle, which asks for more time to make electron reach to the surface of a particle where recombination occurs. Therefore, the effect of the added nanoparticle on recombination becomes offset as a consequence of the combination between the slower electron transport in a particle and more sensitive electron transfer at surface of a particle.

The improved electron transport (R_t) ascribed to the widened necks would give an impact on power conversion efficiency of DSCs. As shown in Fig. 10, DSCs based on Mix10 and Mix20 photoanodes showed better power conversion performance than that based Aggregate photoanode with an increased short circuit current density (J_{sc}), as the denser structure of Mix10 and Mix20 films increased surface areas for more dye loading [17]. If the added nanoparticles were used entirely in filling the gaps between adjacent aggregates, it can be assumed that 10 wt.% of the nanoparticles added would generate additional 10% increase in the surface area and corresponding J_{sc} (LHE). However, when 10 wt.% of the nanoparticles were added, the improvement of J_{sc} by 26% was obtained, suggesting that the increased J_{sc} must be ascribed to the improvement of both charge collection and light harvesting. Falling back in the photocurrent occurring when 20 wt.% of nanoparticles was added seemed to be a result of the compromise between the increased surface area and the reduced light scattering effect, as discussed in Fig. 5 [33].

4. Conclusions

The added TiO_2 nanoparticles gave two impacts on the morphological aspects of the TiO_2 aggregate film; widened necks by preferentially filling vacant space around necks between adjacent TiO_2 aggregates and increased surface area as a result of the denser film. The transport resistance (R_t) was found to be reduced with adding the TiO_2 nanoparticles, indicating that facile transfer of electron from one aggregate to the other occurs through the fortified necks. However, the necks and gaps filled with the TiO_2 nanoparticles showed diminished scattering effect of the film (reflectance) as a result of reduction of scattering centers such as necks and gaps. As the other morphological change, the increased surface area with adding the TiO_2 nanoparticles improved absorbance of the sensitized film. From the compensated characteristics of the film among R_t, reflectance and absorbance with adding the TiO_2 nanoparticles, Mix10 showed the highest photocurrent and resulting efficiency, suggesting good strategy to achieve further improvement of DSCs' performances by employing light scattering centers such as aggregate and scattering layer whose connections are improved for better electron movement.

Acknowledgments

Most of the synthesis of nanostructures and electrical characterization was supported by the National Science Foundation (DMR-1035196) (K.S.P.), and some detailed structural characterization was been supported in part by the US Department of Energy, Office of

Basic Energy Sciences, Division of Materials and Engineering under Award No. DE-FG02-07ER46467 (Q.F.Z.). JTX would also like to acknowledge the fellowship from the China Scholarship Council.

References

[1] B. O'Regan, M. Grätzel, A low-cost, high-efficiency solar cell based on dye-sensitized colloidal TiO_2 films, Nature 353 (1991) 737.
[2] G.K. Mor, K. Shankar, M. Paulose, O.K. Varghese, C.A. Grimes, Use of highly-ordered TiO_2 nanotube arrays in dye-sensitized solar cells, Nano Lett. 6 (2006) 215.
[3] A. Kay, M. Grätzel, Dye-sensitized core–shell nanocrystals: improved efficiency of mesoporous tin oxide electrodes coated with a thin layer of an insulating oxide, Chem. Mater. 14 (2002) 2930.
[4] M.K. Nazeeruddin, A. Kay, I. Rodicio, R. Humphrybaker, E. Muller, P. Liska, N. Vlachopoulos, M. Grätzel, Conversion of light to electricity by cis-X2bis(2,2′-bipyridyl-4,4′-dicarboxylate)ruthenium(II) charge-transfer sensitizers(X = Cl-, Br-, I-, CN-, and SCN-) on nanocrystalline titanium dioxide electrodes, J. Am. Chem. Soc. 115 (1993) 6382.
[5] G.J. Meyer, The 2010 millennium technology grand prize: dye-sensitized solar cells, ACS Nano 4 (2010) 4337.
[6] A. Usami, Theoretical study of application of multiple scattering of light to a dye-sensitized nanocrystalline photoelectrochemical cell, Chem. Phys. Lett. 277 (1997) 105.
[7] J. Ferber, J. Luther, Computer simulations of light scattering and absorption in dye-sensitized solar cells, Sol. Energy Mater. Sol. Cells 54 (1998) 265.
[8] S. Hore, C. Vetter, R. Kern, H. Smit, A. Hinsch, Influence of scattering layers on efficiency of dye-sensitized solar cells, Sol. Energy Mater. Sol. Cells 90 (2006) 1176.
[9] F.T. Kong, S.Y. Dai, K.J. Wang, Review of recent progress in dye-sensitized solar cells, Adv. OptoElectron. 75384 (2007).
[10] Q.F. Zhang, T.P. Zhou, B. Russo, S.A. Jenekhe, G.Z. Cao, Aggregation of ZnO nanocrystallites for high conversion efficiency in dye-sensitized solar cells, Angew. Chem. Int. Ed. 47 (2008) 2402.
[11] K. Park, Q.F. Zhang, B.B. Garcia, X.Y. Zhou, Y.-H. Jeong, G.Z. Cao, Effect of an ultrathin TiO_2 layer coated on submicrometer-sized ZnO nanocrystallite aggregates by atomic layer deposition on the performance of dye-sensitized solar cells, Adv. Mater. 22 (2010) 2329.
[12] S.R. Gajjela, C. Yap, P. Balaya, Multi-functional photoanode films using mesoporous TiO_2 aggregate structure for efficiency dye sensitized solar cells, J. Mater. Chem. 22 (2012) 10873.
[13] S.H. Kang, S.-H. Choi, M.-S. Kang, J.-Y. Kim, H.-S. Kim, T. Hyeon, Y.-E. Sung, Nanorod-based dye-sensitized solar cells with improved charge collection efficiency, Adv. Mater. 20 (2008) 54.
[14] L. Yang, W.W.-F. Leung, Electrospun TiO_2 nanorods with carbon nanotubes for efficient electron collection in dye-sensitized solar cells, Adv. Mater. 25 (2013) 1792.
[15] P. Docampo, S. Guldin, U. Steiner, H.J. Snaith, Charge transport limitations in self-assembled TiO_2 photoanodes for dye-sensitized solar cells, J. Phys. Chem. Lett. 4 (2013) 698.
[16] K. Park, J.T. Xi, Q.F. Zhang, G.Z. Cao, Charge transport properties of ZnO nanorod aggregate photoelectrodes for DSCs, J. Phys. Chem. C 116 (2011) 20992.
[17] J.T. Xi, Q.F. Zhang, K. Park, Y.M. Sun, G.Z. Cao, Enhanced power conversion efficiency in dye-sensitized solar cells with TiO_2 aggregates/nanocrystallites mixed photoelectrodes, Electrochim. Acta 56 (2011) 1960.
[18] P. Joshi, L. Zhang, D. Davoux, Z. Zhu, D. Galipeau, H. Fong, Q. Qiao, Composite of TiO_2 nanofibers and nanoparticles for dye-sensitized solar cells with significantly improved efficiency, Energy Environ. Sci. 3 (2010) 1507.
[19] W. Chen, Y. Qiu, Y. Zhong, K. Wong, S. Yang, High-efficiency dye-sensitized solar cells based on the composite photoanodes of SnO_2 nanoparticles/ZnO nanotetrapods, J. Phys. Chem. A 114 (2010) 3127.
[20] J. Bisquert, Theory of the impedance of electron diffusion and recombination in a thin layer, J. Phys. Chem. B 106 (2002) 325.
[21] R. Kern, R. Sastrawan, J. Ferber, R. Stangl, J. Luther, Modeling and interpretation of electrical impedance spectra of dye solar cells operated under open-circuit conditions, Electrochim. Acta 47 (2002) 4213.
[22] T. Hoshikawa, R. Kikuchi, K. Eguchi, Impedance analysis for dye-sensitized solar cells with a reference electrode, J. Electroanal. Chem. 588 (2006) 59.
[23] T. Hoshikawa, M. Yamada, R. Kikuchi, K. Eguchi, Impedance analysis of internal resistance affecting the photoelectrochemical performance of dye-sensitized solar cells, J. Electrochem. Soc. 152 (2005) E68.
[24] F. Fabregat-Santiago, J. Bisquert, G. Garcia-Belmonte, G. Boschloo, A. Hagfeldt, Influence of electrolyte in transport and recombination in dye-sensitized solar cells studied by impedance spectroscopy, Sol. Energy Mater. Sol. Cells 87 (2005) 117.
[25] Q. Wang, S. Ito, M. Grätzel, F. Fabregat-Santiago, I. Mora-Seró, J. Bisquert, T. Bessoho, H. Imai, Characteristics of high efficiency dye-sensitized solar cells, J. Phys. Chem. B 110 (2006) 25210.
[26] Q. Wang, J.-E. Moser, M. Grätzel, Electrochemical impedance spectroscopic analysis of dye-sensitized solar cells, J. Phys. Chem. B 109 (2005) 14945.
[27] J.R. Jennings, Q. Wang, Impedance spectroscopy of dye-sensitized solar cells: analysis of measurement and fitting errors, J. Electrochem. Soc. 159 (2012) F141.
[28] C.-P. Lee, P.-Y. Chen, R. Vittal, K.-C. Ho, Iodine-free high efficient quasi solid-state dye-sensitized solar cell containing ionic liquid and polyaniline-loaded carbon black, J. Mater. Chem. 20 (2010) 2356.
[29] Z. Yang, T. Chen, R. He, H. Li, H. Lin, L. Li, G. Zou, Q. Jia, H. Peng, A novel carbon nanotube/polymer composite film for counter electrodes of dye-sensitized solar cells, Polym. Chem. 4 (2013) 1680.
[30] J. Bisquert, A. Zaban, M. Greenshtein, I. Mora-Seró, Determination of rate constants for charge transfer and the distribution of semiconductor and electrolyte electronic energy levels in dye-sensitized solar cells by open-circuit photovoltage decay method, J. Am. Chem. Soc. 126 (2004) 13550.
[31] J.W. Ondersma, T.W. Hamann, Measurements and modeling of recombination from nanoparticle TiO_2 electrodes, J. Am. Chem. Soc. 133 (2011) 8264.
[32] A. Hagfeldt, G. Boschloo, L. Sun, L. Kloo, H. Pettersson, Dye-sensitized solar cells, Chem. Rev. 110 (2010) 6595.
[33] S. Hore, P. Nitz, C. Vetter, C. Prahl, M. Niggemann, R. Kern, Scattering spherical voids in nanocrystalline TiO_2-enhancement of efficiency in dye-sensitized solar cells, Chem. Commun. 15 (2005) 2011.